JOURNAL OF GEOPHYSICAL RESEARCH, VOL. 91, NO. B12, PAGES 12,572-12,586, NOVEMBER 10, 1986

EARTHQUAKE PROCESSES IN THE RAINBOW MOUNTAIN–FAIRVIEW PEAK–DIXIE VALLEY, NEVADA, REGION 1954–1959

Diane I. Doser [1]

Seismological Laboratory, California Institute of Technology, Pasadena

Abstract. The 1954 Rainbow Mountain-Fairview Peak-Dixie Valley, Nevada, sequence produced the most extensive pattern of surface faults in the intermountain region in historic time. Five earthquakes of $M>6.0$ occurred during the first 6 months of the sequence, including the December 16, 1954, Fairview Peak ($M=7.1$) and Dixie Valley ($M=6.8$) earthquakes. Three $5.5 \leq M \leq 6.5$ earthquakes occurred in the region in 1959, but none exhibited surface faulting. The results of the modeling suggest that the $M>6.5$ earthquakes of this sequence are complex events best fit by multiple source-time functions. Although the observed surface displacements for the July and August 1954 events showed only dip-slip motion, the fault plane solutions and waveform modeling suggest the earthquakes had significant components of right-lateral strike-slip motion (rakes of -135° to -145°). All of the earthquakes occurred along high-angle faults with dips of 40° to 70°. Seismic moments for individual subevents of the sequence range from 8.0×10^{17} to 2.5×10^{19} N m. Stress drops for the subevents, including the Fairview Peak subevents, were between 0.7 and 6.0 MPa.

Introduction

The Rainbow Mountain, Fairview Peak, and Dixie Valley, Nevada, earthquakes of 1954 represent one of three normal fault earthquake sequences (the 1959 ($M_S=7.5$) Hebgen Lake, Montana, and the 1983 ($M_S=7.3$) Borah Peak, Idaho, sequences are the others) with $M>7.0$ that have occurred in the intermountain region for which sufficient geodetic, as well as seismic, data are available to determine subsurface fault geometry. Knowledge of subsurface geometry is important in evaluating seismic hazards from normal faults and provides information on deformation at shallow depths in the crust. It is also useful in determining whether older zones of weakness are being reactivated during current earthquake cycles, or whether new fracture systems are developing.

Seismic reflection profiles to depths of 10 to 15 km [Smith and Bruhn, 1984; Anderson et al., 1983; Allmendinger et al., 1983] have shown the existence of listric faults and detachment surfaces throughout the Great Basin; however, studies of the Borah Peak [Stein and Barrientos, 1985; Doser and Smith, 1985] and Hebgen Lake [Doser, 1985] earthquake sequences indicate that the large earthquakes of these sequences occurred on planar, high-angle normal faults. The studies indicate that the earthquakes had simple source-time functions and nucleated near the base of the seismogenic zone. Low stress drops (< 15 MPa) were also associated with these events.

We have used teleseismic body wave modeling and short-period first-motion data to determine subsurface fault orientation for nine earthquakes occurring between 1954 and 1959. Our analysis indicates that all of these earthquakes occurred along high-angle faults extending to maximum depths of 12 to 15 km, although several of the faults may change orientation with depth. Source-time functions determined in the modeling process exhibit complexities not seen in the Hebgen Lake or Borah Peak earthquake sequences. We compare our estimates of fault orientations from seismic information with the recent geodetic models of Snay et al. [1985], and a study of long-period surface waves of the Fairview Peak and Dixie Valley earthquakes (D. I. Doser and H. Kanamori, unpublished manuscript, 1986), and the surface faulting observed by Tocher [1956] and Slemmons [1957]. We finally discuss possible geologic features that may influence faulting in the region.

Regional Setting

The Rainbow Mountain-Fairview Peak-Dixie Valley region (hereafter referred to as the Fairview Peak region) is located in the west-central portion of the Basin and Range province (Figure 1). Our study area extends from about 117° 45′ W to 119° 15′ W and 39°N to 40°N (Figure 1) to include several earthquakes in the southwestern corner of the area that occurred in 1959. The surface faulting depicted in Figure 1 occurred during 1954.

The Stillwater Range (Figure 1) is the major feature in the center of the study area. The range consists of Mesozoic pelites, gabbros, and granodiorites overlain by a Tertiary volcaniclastic sequence and basalts [Okaya and Thompson, 1985]. West of the Stillwater Range lie the Quaternary and lacustrine deposits of the Carson Sink. Seismic reflection profiles [Hastings, 1979] show 2-3 km of alluvium under the Carson Sink, as well as a major range front fault beginning 10 km east of the northern end of the Rainbow Mountain fault and running northward along the northwestern side of the Stillwater Range. South of the Carson Sink this fault dies out into westward tilting sediments that lie against eastward dipping faults of the Rainbow Mountain fault zone. The Rainbow Mountain fault zone bounds a buried horst beneath the youngest valley fill [Hastings, 1979]. Seismic reflection data suggest that the eastward dipping faults of the Rainbow Mountain fault zone are of large displacement, but not as large as along the westward dipping fault bounding the Stillwater Range to the north [Anderson et al., 1983].

The eastern side of the Stillwater Range is bounded by the eastward dipping Dixie Valley fault. Okaya and Thompson [1985] used seismic reflection profiles and gravity data across Dixie Valley to show that Dixie Valley is an asymmetrical graben filled with about 1.8 km of lacustrine and alluvial fan material, and is bounded on the east by a number of minor high-angle faults that dip to the west. No major fault appears to separate Dixie Valley from the Clan Alpine Mountains [Okaya and Thompson, 1985]. Based on a number of geologic and geophysical constraints, Okaya and Thompson [1985] believe that the Dixie Valley fault is a steeply dipping planar fault and favor a model of magmatic intrusion to produce the high-angle fault system seen in the reflection section. Smith [1968] estimates that 2-3 km of right lateral offset have occurred along the Dixie Valley fault based on an interpretation of aeromagnetic data. Okaya and Thompson [1985] have calculated an

[1] Now at Department of Geological Sciences, University of Texas at El Paso.

Paper number 6B5993.
0148-0227/86/006B-5993$05.00

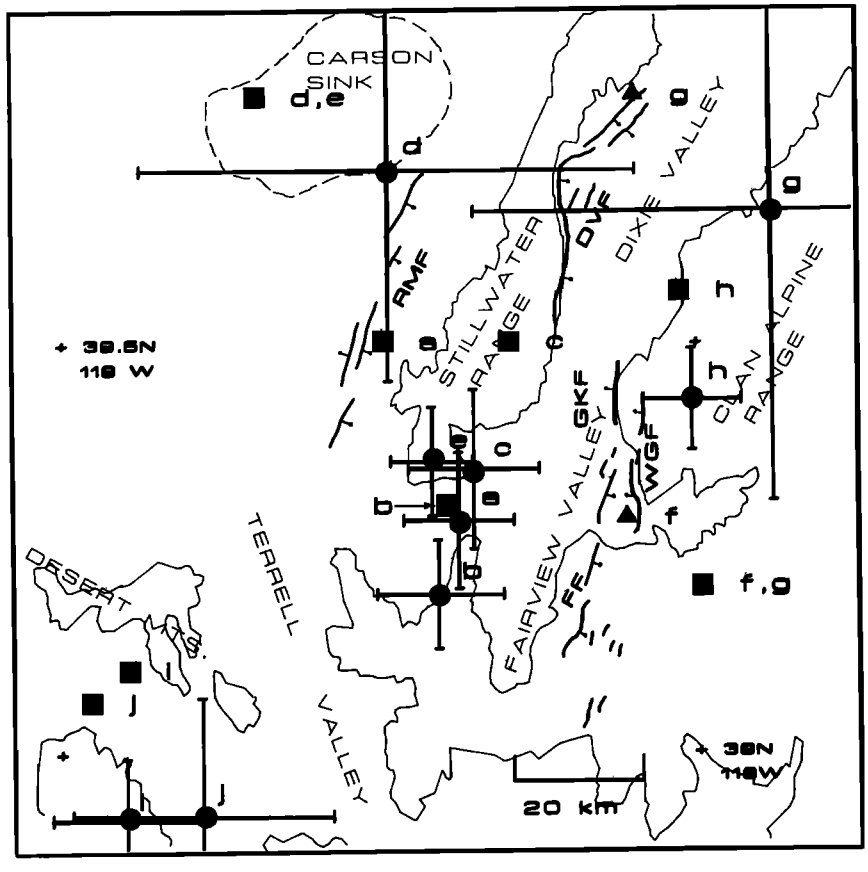

Fig. 1. Earthquake locations (M>5.5) for 1954-1959 and surface faulting during 1954. Letters are keyed to earthquakes listed in Table 1. Surface fault traces of the 1954 sequence are modified from Romney [1957]. Squares denote ISS locations. Triangles denote Romney's [1957] relocations of the Dixie Valley and Fairview Peak earthquakes. Circles are relocations relative to ISS epicenter for the Fairview Peak earthquake (the square f). Error bars represent the 95% confidence intervals for individual locations. Balls show the downthrown side of normal faults. RMF is the Rainbow Mountain fault, DVF is the Dixie Valley fault, FF is the Fairview fault, GKF is the Gold King fault, and WGF is the West Gate fault. Thin solid lines indicate the 5000-ft contour interval. A thin dashed line encloses the Carson Sink.

extension rate of 0.38 mm/yr across the valley over a period of 8 m.y.

South of Dixie Valley and east of Fairview Valley is the Fairview-Gold King-West Gate fault system. The Fairview fault dips eastward, while the West Gate fault dips westward, the two faults thus forming a graben along the north-central part of the fault system. The West Gate fault bounds the southern end of the Clan Alpine Range. Although the Gold King fault lies along strike and 5 km north of the end of the Fairview fault, it dips to the west. Slemmons et al. [1959] show evidence for a 1903 event, the Wonder earthquake, along the Gold King fault.

In the southwestern corner of the study area, Slemmons [1956] notes a northwest striking fault of late Quaternary age that probably dips to the east. Surface faulting was not reported in this region during the 1954-1959 sequence.

Data and Methods

Data from a number of sources were used to determine the subsurface fault geometry and rupture processes of the Rainbow Mountain-Fairview Peak-Dixie Valley sequence. In this section we discuss the methods that were used to relocate earthquakes, determine focal mechanisms from first-motion data, and model teleseismic waveforms. We also review the data available from previous geologic and geodetic studies.

Earthquake Locations

Ten earthquakes with M>5.5 occurred in the Fallon region between 1954 and 1959 (Table 1). Figure 1 shows the locations of these 10 events determined by the International Seismological Summary (ISS). Magnitudes listed in Table 1 are magnitude values most commonly quoted in the literature and are without reference to the magnitude scale used.

In an effort to improve the quality of the locations, we relocated the earthquakes using a master event technique, rather than a joint hypocenter determination, because we felt that a joint hypocenter approach would sacrifice well-recorded events in an attempt to locate the poorly recorded events of the sequence. There has not been an earthquake in the region that has been large enough to be well recorded at regional and teleseismic distances since 1959, so we chose the Fairview Peak earthquake (event f) as our master event. This earthquake was recorded by the largest number of stations and had the greatest number of impulsive arrivals at distances $< 30°$. Romney [1957] located the epicenter for the Fairview Peak earthquake less than 3

TABLE 1. Earthquake Locations and Focal Mechanisms

Event	Date	Origin Time, UT	Fault Zone*	M	ISS Location	Relocation	Strike,Dip,Rake+
a	July 6, 1954	1113	RM	6.6	39.5 -118.5	39.29 -118.36	336,78,-140
b	July 6, 1954	2207	RM	6.4	39.3 -118.4	39.20 -118.40	348,70,-157
c	Aug. 24, 1954	0551	RM	6.8	39.5 -118.3	39.35 -118.34	355,51,-145 (33,40,-90)
d	Aug. 31, 1954	2220	RM	5.8	39.8 -118.7	39.72 -118.47	0,58,-162
e	Sept. 1, 1954	0518	RM?	5.5	39.8 -118.7	39.36 -118.40	20,70,-42
f	Dec. 16, 1954	1107	F	7.1	39.2 -118.0	39.20 -118.00 (fixed)	350,60,-150
g	Dec. 16, 1954	1111	DV	6.8	39.2 -118.0	39.67 -117.87	
h	March 23, 1959	0710	DV?	6.3	39.56 -118.03	39.43 -117.99	348,46,-168
i	June 23, 1959	1435	?	6.0	39.10 -118.90	38.92 -118.89	310,68,-148
j	June 23, 1959	1504	?	5.5	39.06 -118.96	38.93 -118.77	

*RM, Rainbow Mountain; F, Fairview; and D, Dixie Valley.
+Assuming eastward dipping nodal plane is fault plane.

km east of the Fairview fault scarp (Figure 1), a location that appears to be too close to the fault if the earthquake began at a depth of 10-15 km, the normal depth range for microearthquakes in the region [Stauder and Ryall, 1967]. The ISS epicenter is located about 15 km from the Fairview fault. This location is more consistent with the probable focal depth of the earthquake. Therefore we have chosen this location for the calculation of station delays used in the master event technique. Delays were calculated for stations with $\Delta < 30°$, and stations with delays greater than 3 s were not used in the later relocations. P arrivals were read from the original seismograms for stations in southern California and from film copies of seismograms for several other western U. S. stations. ISS readings were used only if the arrivals were noted as impulsive and were recorded on vertical seismometers. Focal depths were fixed at 12 km, and the Herrin [1968] velocity model was used.

Relocations obtained in this process are shown with error bars in Figure 1. The error bars show the 95% confidence intervals [Flinn, 1965] obtained when each event was relocated after correcting arrival times for station delays determined from the master event. The error bars do not include errors associated with the master event location, which are estimated to be ± 7 km in a north-south direction and ± 9 km in an east-west direction. Note that the relocated epicenters correlate well with their associated surface-scarps.

Focal Mechanisms

Focal mechanisms have been published for three earthquakes (July 6 main shock(a), August 24 main shock(c), and Fairview Peak(f)) of the 1954-1959 sequence [Fara, 1964; Wickens and Hodgson, 1967]. We have reevaluated these three solutions and determined solutions for an additional five events. First motions were read from the seismograms used in relocating the earthquakes ($\Delta < 30°$) as well as from seismograms recorded at teleseismic distances. First-motion information from the ISS listings was used only when the motion was noted as having been read from a vertical seismometer. We assumed a focal depth of 12 km in the mechanism deteminations. Equal-area lower hemisphere projections of our solutions are shown in Figures 2 and 3, and the solutions are listed in Table 1.

Body Wave Modeling

Body waves at distances of 50°-80° were modeled to obtain additional details of the source mechanism as well as focal depth and source time function. Only five events (a,b,c,f,g) had large enough amplitudes to be well recorded at these distances. Although the entire sequence occurred before the establishment of the worldwide standardized network of seismograph stations, a number of stations around the world were operating Galitzin seismograph systems with seismometer periods of 10 to 24 s and magnifications of 700-1100. We collected seismograms from seven stations, including five European stations (COP,TRS,PAR,UCC), and one each from Greenland (SCO), Bolivia (LPZ), and Japan (ABU). This station distribution necessitated the modeling of radial P and SH, in addition to vertical P, to obtain a satisfactory data set.

The forward modeling process follows the method of Langston and Helmberger [1975]. We generated starting models for the modeling process using the focal mechanisms obtained from first-motion data, with a depth of 12 km. An estimate of the starting source-time function was based on the observed width of the first several cycles of P or S phases at a station. Quality of fit was determined by cross correlation of the data and synthetics. Figures 4 through 9 show the results of the modeling process.

Seismograms for several earthquakes of the sequence showed a distinct change in shape 8 to 15 s after the initial P arrival, as in Figure 4. To determine whether the secondary arrivals were later subevents, the first portion of the observed P and S waveforms were modeled and then the best fit synthetics were subtracted from the observed seismograms. The shape of the resulting waveforms appeared consistent with the arrivals of later subevents. Under this hypothesis, entire seismograms could be successfully modeled as indicated in Figure 4. Initially we assumed that succeeding subevents had the same focal mechanism and focal depth as the first subevent for a particular earthquake. This process worked well, except for the July 6 main shock (event a), where a mismatch suggested that the second subevent had a much different focal mechanism and depth than the first subevent.

Source parameters and error estimates from the modeling process are shown in Table 2. For the majority of the earthquakes studied, the European stations were located in strategic positions on the focal sphere. Small pertubations in focal mechanism produced large variations in waveform shape, enabling us to obtain an accuracy of up to ±2° in determining the focal mechanism. The source-time function width generally could be perturbed by 0.5 s without producing variations in waveform shape, and the focal depth could be perturbed by 1 to 3 km.

The rupture length, L, in Table 2 was estimated from

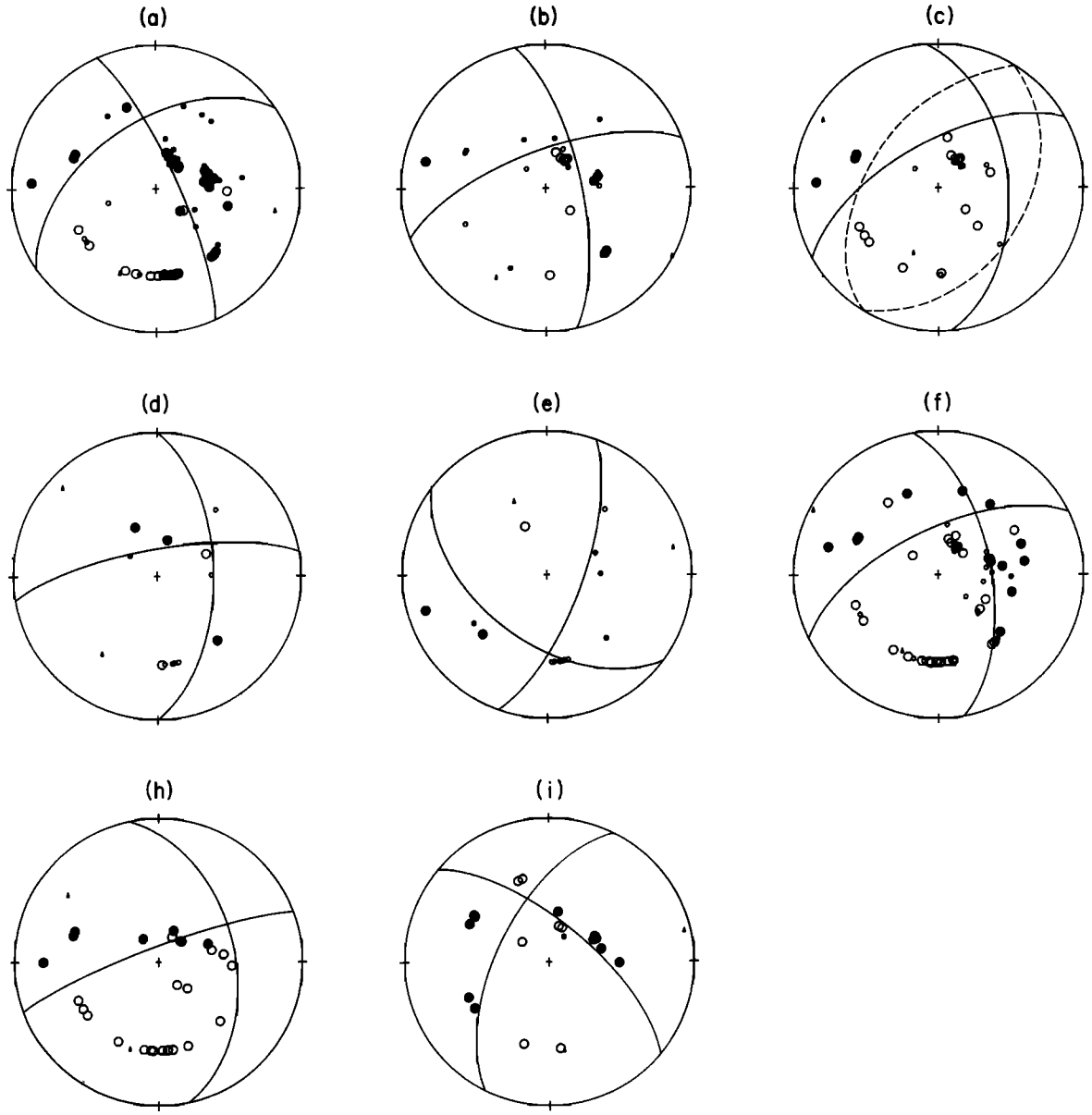

Fig. 2. Focal mechanisms for earthquakes in the Rainbow Mountain-Fairview Peak-Dixie Valley earthquake sequence. The mechanisms are equal-area, lower hemisphere projections, with open circles denoting dilatation and solid circles compression. Smaller circle size denotes emergent first motion. An alternate focal mechanism for event c is shown by the dashed lines. Letters are keyed to the earthquakes listed in Table 1.

t_c=L/v [Kanamori and Stewart, 1976], where t_c is the rupture time (rise time + plateau time) and v is the rupture velocity (chosen to be 3.5 km/s).

Moment magnitude ($\hat{M}$) was estimated using the relationship log $\hat{M}$=2/3 log M_o^s -10.7 [Hanks and Kanamori, 1979], where M_o^s is the seismic moment obtained from body wave modeling (Table 2). The moment magnitudes for events a, b, and c were 0.3 to 0.5 magnitude units smaller than commonly quoted magnitudes. Consequently M_S magnitudes were estimated for these three events, and M_S values of 6.1 (event a), 5.9 (event b), and 6.5 (event c) agree well with the moment magnitudes. The disparity between commonly quoted magnitudes and moment magnitudes demonstrates the necessity of recomputing magnitudes of older earthquake sequences before making source parameter comparisons with other earthquakes.

Stress drops (Table 2) for the 1954-1959 earthquakes were estimated for a rectangular fault model using $\Delta\sigma$=8 M_o /3π W^2 L [Starr, 1928], where W is the fault width, and L is the fault length. All earthquakes studied had stress drops of less than 6.0 MPa. These values support Cloud's [1957] observation that, except for the spectacular surface faulting, the maximum intensity in the epicentral area for events of the sequence did not exceed Modified Mercalli VIII. Stress drops for the Hebgen Lake and Borah Peak earthquakes are 11.5 and 1.2-1.7 MPa, respectively [Doser, 1985; Doser and Smith, 1985], suggesting that large normal fault events in the intermountain region may have low

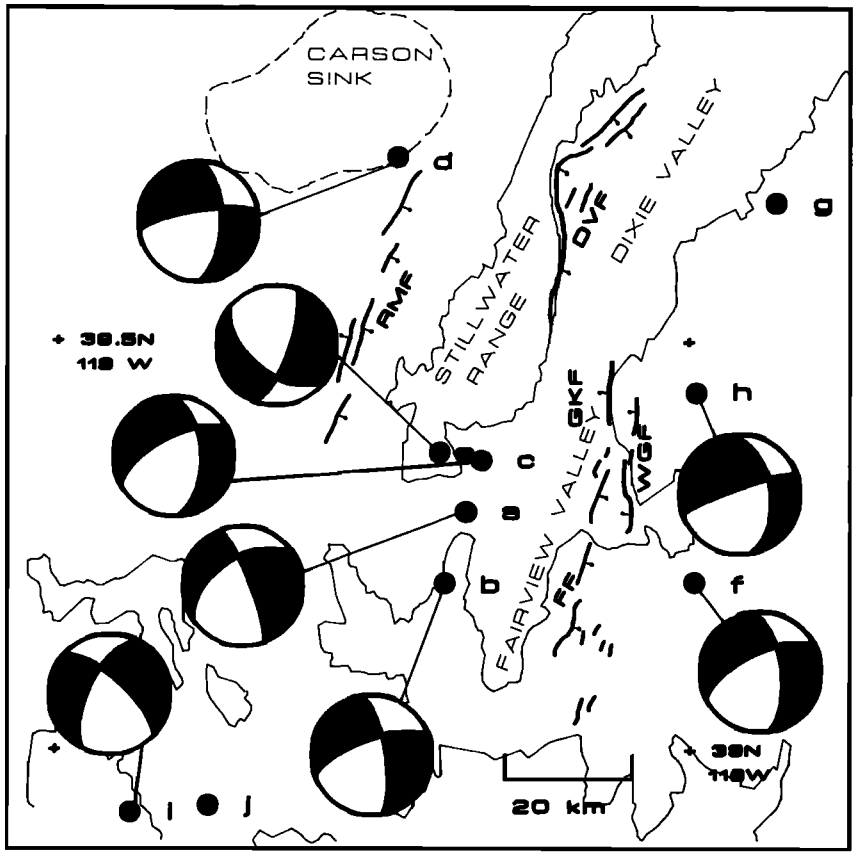

Fig. 3. Focal mechanisms (1954-1959) and surface faulting. White areas on focal spheres indicate dilatation.

stress drops when compared with events of similar magnitude in other regions.

Geologic Data

Surface faulting was produced during the July 6, 1954, Rainbow Mountain (event a) earthquake, the August 24, 1954, Rainbow Mountain (event c) earthquake, and the December 16, 1954, Fairview Peak (event f) and Dixie Valley (event g) earthquakes (Figure 1). Table 3 lists the fault parameters obtained from the geologic studies of Tocher [1956] and Slemmons [1957].

Geologic moment, M_o^g, for each fault segment (Table 3) was estimated from the relationship $M_o^g = \mu$ w L $\bar{s}$, where μ is the shear modulus, w the fault width (assuming a 60° fault dip and the focal depth obtained from body wave modeling), $\bar{s}$ the average slip, and L the fault length (Table 3). For fault segments with slip $>$ 1 m, M_o^g was estimated using the length of the fault with slip $>$ 1 m.

Geodetic Data

Leveling and triangulation surveys conducted in the region between 1934 and 1967 provide important geodetic constraints to the study of the earthquake source processes. Savage and Hastie [1969] use the results of triangulation surveys in 1954 and 1955 [Whitten, 1957] to obtain a dislocation model for the Fairview Peak earthquake. Their model parameters are listed in Table 4.

More recently, Snay et al. [1985] have reevaluated the geodetic data, including a survey in 1935, to obtain a model of faulting for the entire Fairview Peak region. Fault parameters obtained for their best fit model, a model composed of five faults (Rainbow Mountain, Fairview (deep), Fairview (shallow), Gold King-West Gate, and Dixie Valley), and an alternative model containing a sixth hypothetical fault are listed in Table 4.

Results

July 6, 1954 (1113 UT) (Event a)

The first earthquake of the Rainbow Mountain sequence on July 6, 1954 (event a), produced about 15 km of surface faulting along the southern end of the Rainbow Mountain fault with a dip-slip offset of 15 cm [Tocher, 1956]. Our relocation suggests that the rupture began at the extreme southern end of the fault and that rupture propagated northeastward.

The focal mechanism for the July 6 earthquake is essentially the same as the solutions found earlier by Fara [1964] and Wickens and Hodgson [1967], showing right-lateral oblique slip along a fault plane striking 20-30° west of the surface faulting (Figures 2 and 3). Note that strike-slip motion was not observed along the surface trace of the Rainbow Mountain fault [Tocher, 1956]. Studies of geodetic data by Meister et al. [1968] and Snay et al. [1985], however, are consistent with right-lateral strike-slip motion across the Rainbow Mountain fault.

The first subevent of the July 6 main shock (Figure 4) was best modeled as having the same focal mechanism as the first-motion solution with a significant component of right-lateral strike-slip motion and a focal depth of 10 km. The second subevent had a focal mechanism showing

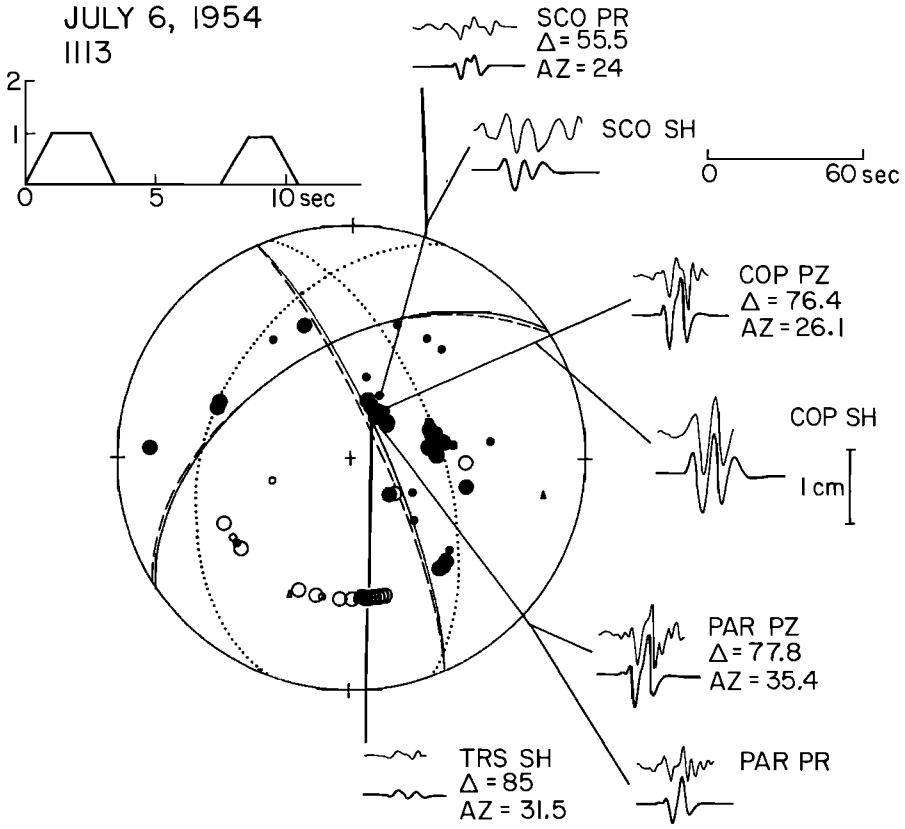

Fig. 4. Body waves of the July 6, 1954 (1113), main shock (event a). Observed (upper) and synthetic (lower) seismograms are shown for each station. First-motion data and the first-motion focal mechanism (solid lines) are shown for reference. The dashed lines are the focal mechanism for the first subevent, and the dotted lines are the mechanism for the second subevent. The source-time function is shown at the top. The horizontal scale shows the relative heights of the subevent source-time functions. Δ is the epicentral distance, and Az is the station azimuth. All seismograms on this and the following figures have been normalized to a magnification of 1000 for comparison purposes. PZ is the vertical P component, PR the radial P component, and SH the transverse S component.

predominately dip-slip motion and a focal depth of 7 km. The complexity of this event may explain the discrepancy between the surface faulting, geodetic, and first-motion information. It appears that the greatest moment during this earthquake was generated along a deeper fault with a component of strike-slip motion detected in the first-motion and geodetic data. The surface faulting may have taken place during the second subevent that had a small component of strike-slip motion that may not have been detected at the surface. The body wave moment (Table 2) for this earthquake is nearly twice the geologic moment (Table 3).

July 6, 1954 (2207 UT) (Event b)

The relocated and ISS epicenter indicate that the second earthquake on July 6 (event b) occurred to the south of the Rainbow Mountain fault scarp. This location correlates well with Tocher's [1956] observation that damage and ground cracking in the region southeast of the Rainbow Mountain fault scarp were greater for the second aftershock. The focal mechanism from first-motion data for this earthquake (Figures 2 and 3) exhibited a larger component of right-lateral strike-slip motion than the main shock (event a).

The July 6 aftershock was the smallest earthquake to be well recorded at teleseismic distances. The waveforms (Figure 5) of the earthquake were simple. The best model for the earthquake was a mechanism with less strike-slip motion than the fault plane solution and only violates three near-nodal first-motion observations. A focal depth of 8 km was obtained.

August 24, 1954 (Event c)

The August 24, 1954, Rainbow Mountain earthquake (event c) ruptured northward along the Rainbow Mountain fault, producing additional displacement along the northern end of the July (event a) fault scarps, and new scarps that extended 20 km to the north. A maximum dip-slip displacement of 75 cm was observed along the August surface rupture [Tocher, 1956]. The relocated epicenter for this event suggests that the rupture may have begun several kilometers to the north of the point of initial rupture for the July 6 (event a) earthquake.

The first-motion data (Figure 2) for this earthquake suggest two possible focal mechanisms. The first mechanism shows right-lateral oblique slip along a fault plane striking 335° and dipping 50° east (solid line, Figure 2). The second mechanism shows pure dip-slip motion along the fault (dashed line, Figure 2). Fara [1964] and Wickens and Hodgson [1967] obtain solutions with right-lateral oblique slip. A composite focal mechanism for microearthquakes of the Rainbow Mountain fault zone [Ryall and

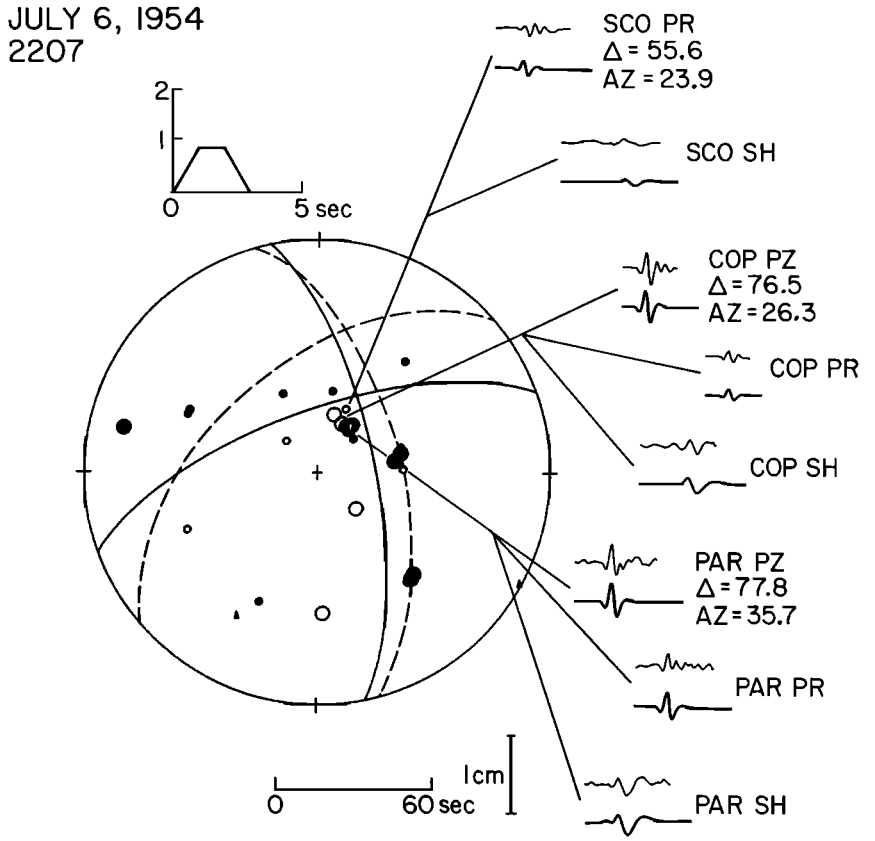

Fig. 5. Body waves for the July 6, 1954, aftershock (event b) at 2207 UT. See Figure 4 for explanation of symbols.

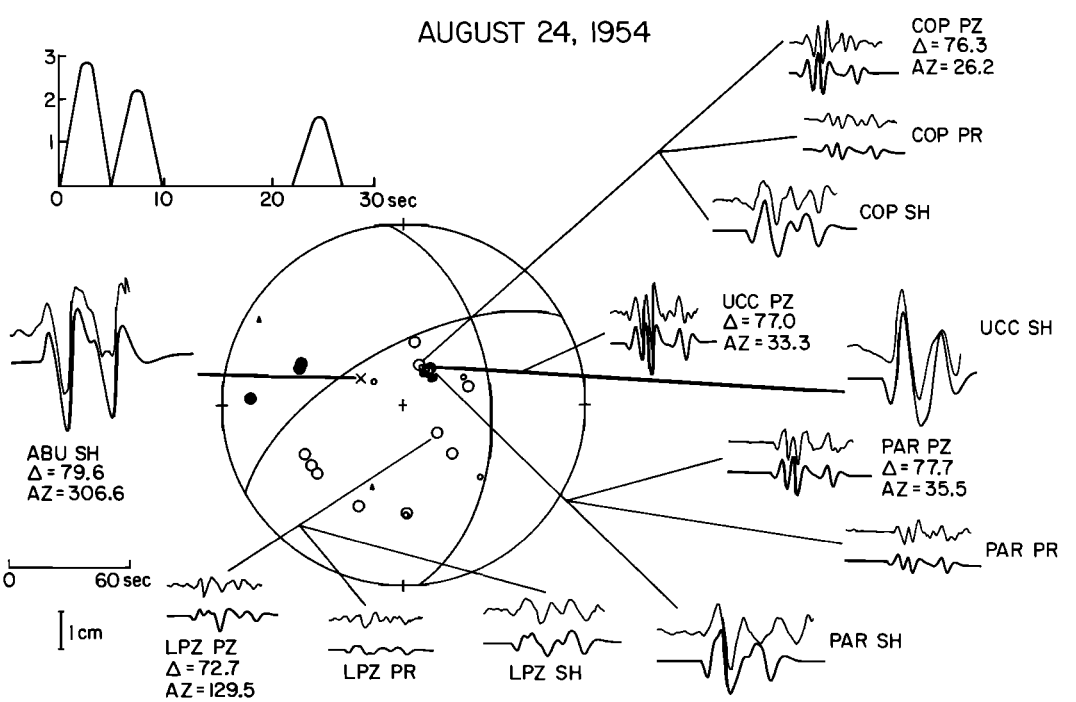

Fig. 6. Body waves from the August 24, 1954, earthquake (event c). See Figure 4 for explanation of symbols. The waveforms are best modeled by a source-time function consisting of three trapezoids. The mechanism determined from body wave modeling is the same as the first-motion mechanism in Figure 2 showing predominately strike-slip motion.

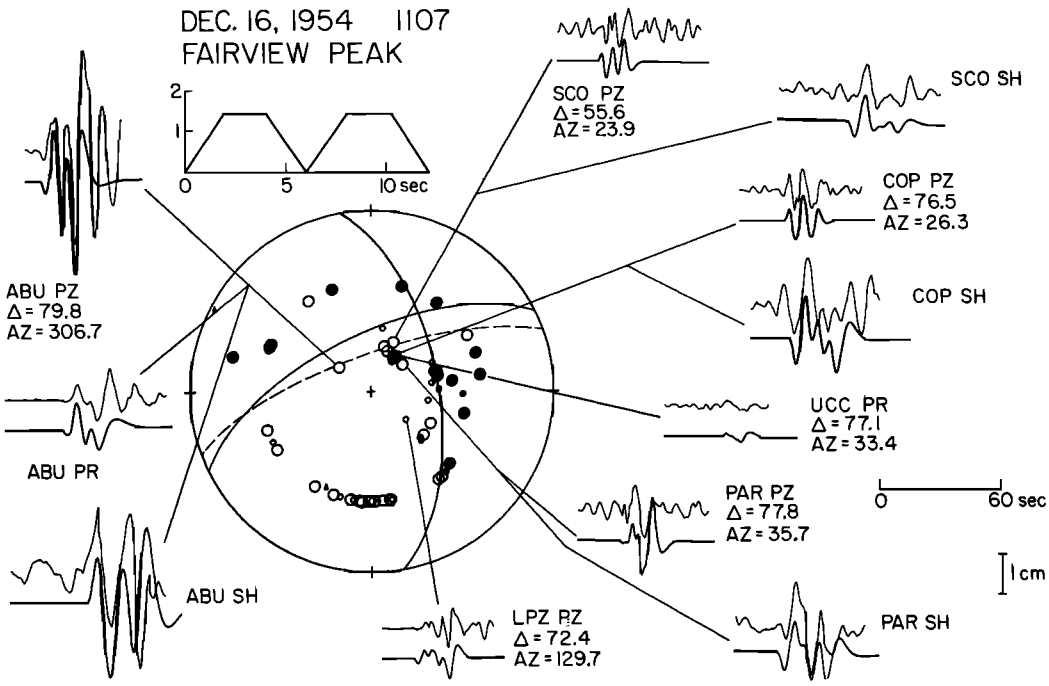

Fig. 7. Body waves from the December 16, 1954 (1107 UT), Fairview Peak (event f) earthquake. Note high-frequency arrivals at SCO PZ, COP PZ, and PAR PZ. The waveforms were modeled by a two-trapezoid source-time function with a mechanism with a 10° greater rake than the first-motion mechanism.

Malone, 1971] is similar to the pure dip-slip mechanism for the August main shock. Body wave modeling supports the right-lateral oblique slip solution.

The August 24 earthquake appears to be one of the most complex events of this sequence. Seismograms of this earthquake (Figure 6) are best modeled as a series of three source-time functions. The waveforms were better modeled by a mechanism with a component of right-lateral strike-slip motion, rather than the dip-slip mechanism also shown in Figure 2. The second subevent occurred immediately after the first subevent, but the third event followed 12 s later. The arrival of the third subevent is seen well on the vertical component seismograms shown in Figure 6. The modeling suggests that rupture in this earthquake began at a deeper point along the Rainbow Mountain fault than the July 6 main shock (12 km versus 10 km). It is possible that the first subevent broke a barrier that stopped rupture during the July 6 main shock. The second and third subevents may represent rupture along the fault to the north of the segment that ruptured in July. The unilateral rupture lengths of 10 km for these subevents correspond well with the two northern segments of the August surface rupture that had lengths of 6 and 10 km. A surveyor who felt this earthquake reported that the earthquake was "a series of three violent quakes, about 15 seconds apart, each lasting for approximately 15 to 20 seconds, and each series was stronger than the one before" [Whitten, 1957]. This description fits the source-time function model well. The timing and duration of the three shocks are different from those obtained by the modeling, but the position of the observer with respect to the events (18 km due east of the northernmost portion of the August surface faulting) may have affected the observation.

The geologic moment (Table 3) was about 30% less than the seismic moment (Table 2) for this earthquake, and the waveform modeling also suggests that some right-lateral strike-slip motion should have been seen at the surface, since the mechanism has nearly equal components of dip-slip and strike-slip motion.

Snay et al. [1985] have attempted to model the geodetic data in the vicinity of the Rainbow Mountain fault. Their best fit (five faults, Table 4) gave a fault length of 112 km and a dip-slip displacement of 5.5 m for the fault, values that would give a much larger moment than expected from the magnitudes of the earthquakes (Table 1) that occurred along this fault system. Their alternative model places a hypothetical westward dipping fault between the Rainbow Mountain and Fairview faults and gives more realistic values for fault length and slip along the Rainbow Mountain fault (six faults, Table 4); however, there is no geologic evidence for the existence of the hypothetical fault. Note that both fault models show right-lateral strike-slip motion along the Rainbow Mountain fault, values consistent with the observed focal mechanisms. Snay et al. conclude that a model with fault slip mechanism may be inadequate to explain all the observed deformation in the region, and suggest magma movement or dike injection as an alternative mechanism. This is exactly the process favored by Okaya and Thompson [1985] to produce the high-angle faults of Dixie Valley.

August 31 and September 1, 1954 (Events d and e)

Two aftershocks (events d and e) of the August main shock (event c) were given the same location at the western end of the Carson Sink by the ISS. Our relocations suggest that the August 31 event occurred near the northern end of the Rainbow Mountain scarp and that the September 1 aftershock may have occurred in the same region as the July 6 (event a) and August 24 main shocks, although the confidence limits for the August 31 aftershock are large.

The August 31 aftershock has a first-motion focal mechanism similar to the July 6 aftershock (event b). The solution is well constrained for the limited number of first-

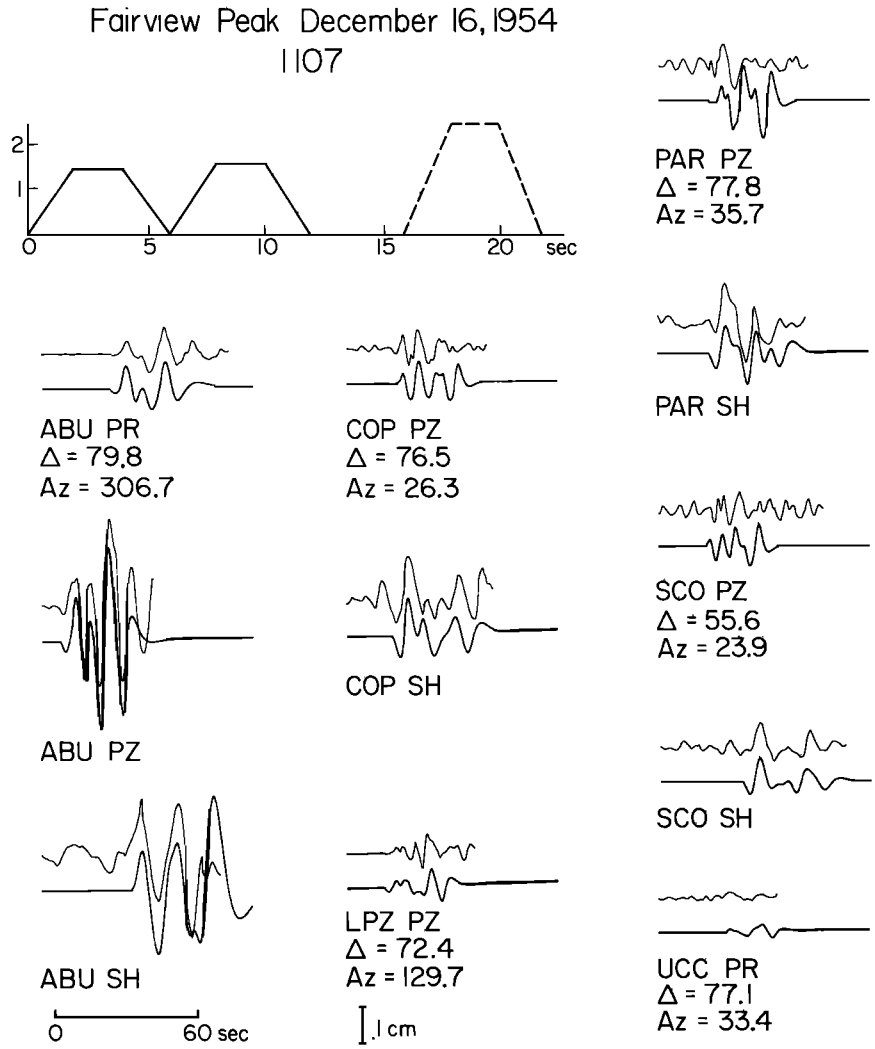

Fig. 8. Body waves from the December 16, 1954, Fairview Peak (event f) earthquake modeled with a source-time function consisting of three trapezoids. This model fits the observed waveforms at SCO SH, COP SH, LPZ PZ, ABU PZ, and ABU PR better than the model shown in Figure 7.

motion polarities available. The focal mechanism from first-motion data for the September 1 aftershock shows a component of left-lateral motion and is unlike any of the other solutions determined in this study. Vetter and Ryall [1983] show several focal mechanisms for post-1977 earthquakes in the Fairview Peak region with components of left-lateral slip, although their solutions show a more northerly strike of the westward dipping nodal plane. Neither aftershock was large enough to produce observable body waves at teleseismic distances.

Meister et al. [1968] studied the strain changes derived from Whitten's [1957] triangulation data and found evidence for east-west extension in the area west of the Rainbow Mountain fault. This suggests dip-slip movement along an unmapped fault. The September 1, 1954, aftershock may have occurred in this area, since its focal mechanism would be consistent with the observed extension rather than with events known to have occurred on the Rainbow Mountain fault.

December 16, 1954 (1107 UT) Fairview Peak (Event f)

The Fairview Peak earthquake occurred 4 min and 20 s before the Dixie Valley earthquake, making it difficult to separate the surface faulting produced by the Fairview Peak earthquake from that produced by the Dixie Valley earthquake. Both the ISS and Romney's [1957] epicenter for the Fairview Peak earthquake (Figure 1) suggest the earthquake began along the Fairview fault system with bilateral rupture along the fault.

Surface scarps extend along the Fairview fault for a distance of 30 km with a maximum dip-slip displacement of 2 m and a maximum right-lateral strike-slip displacement of 3.6 m [Slemmons, 1957]. Eastward dips of 55°-75° were measured for the Fairview fault [Slemmons, 1957]. A 20-km-long scarp with 0.9-1.2 m of dip slip and 0.5-0.9 m of dextral strike-slip motion was produced along the Westgate fault [Slemmons, 1957]. The Gold King fault at the northeastern end of Fairview Valley also ruptured during the earthquake sequence. The fault scarp extended for 10 km along the Gold King fault with about 0.6 m of vertical displacement and little or no strike-slip movement [Slemmons, 1957]. Similar surface rupture was observed for the 1903 Wonder earthquake along the Gold King fault [Slemmons, 1957].

Our fault plane solution (Figures 2 and 3) for the Fairview Peak earthquake is nearly identical to that determined by Romney [1957]. The percentage of right-lateral

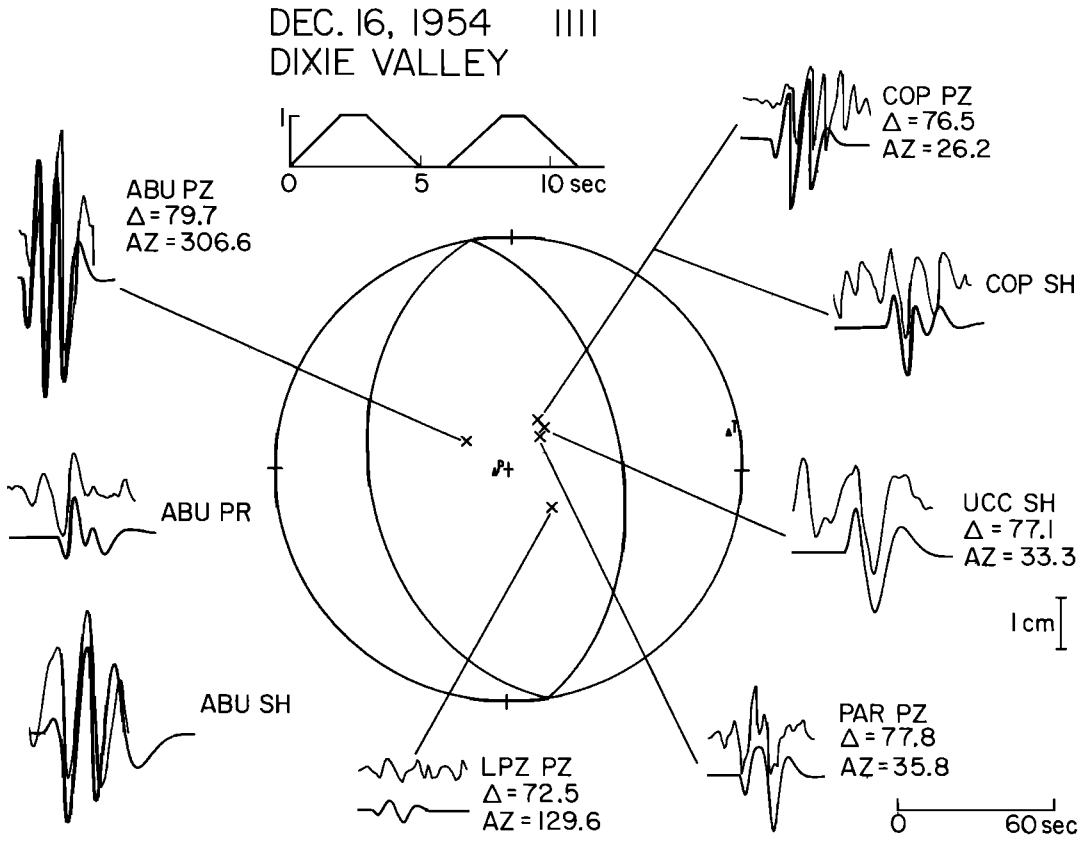

Fig. 9. Body waves from the December 16, 1954 (1111 UT), Dixie Valley (event g) earthquake. Because this event occurred 4 min and 20 s after the Fairview Peak earthquake, first-motion data are unavailable for the Dixie Valley event. The crosses denote station locations on the focal sphere.

motion seen in the solution is equivalent to that seen at the surface. This focal mechanism is similar to the July (event a) and August (event c) main shocks and is consistent with Aki's [1960] observation that the Love waves of these three events were similar.

The fault model obtained for the Fairview fault from geodetic data [Savage and Hastie, 1969] (Table 4) closely matches the surface faulting, rather than the focal mechanism of Romney [1957] or Wickens and Hodgson [1967]. Savage and Hastie noted that their estimate of fault width of 8 km was probably somewhat less than the true fault width. A fault width of 15-16 km is suggested by the microearthquake studies of Stauder and Ryall [1967] and Ryall and Malone [1971]. Ryall and Malone suggest that Savage and Hastie's model reflects the overall trend of a fault zone that is composed of a series of northwest-northeast striking fractures that are consistent with the seismologic information.

Snay et al. [1985] obtained a best fit to the geodetic data by allowing slip along the Fairview fault during the earthquakes to occur along two separate planes. The shallower fault plane (strike 12°, dip 63° E) is similar to Savage and Hastie's model (Table 4) and extends to a depth of 6 km. The deeper fault plane (strike 347°, dip 59° E) extends to a depth of 15-20 km. This model is able to reconcile the difference between the strike of the observed surface faulting and focal mechanisms from first-motion data.

Seismograms for the Fairview Peak earthquake (Figure 7) were noisier than those recorded during the summer months. The earthquake was best modeled as a multiple event with a focal mechanism similar to the first-motion mechanism. Okaya and Thompson [1985] modeled two seismograms of the Fairview Peak earthquake recorded at STU and STR and also obtained a double source-time function for this earthquake, although their second subevent had an amplitude twice that of their first subevent with a duration of 10 s. The duration of their first subevent was the same as the result of this study.

A high-frequency arrival near the beginning of the waveform can be seen on the SCO, COP, and PAR vertical components. This may suggest that the earthquake began with a small, high-frequency event, although other seismograms reproduced by Okaya and Thompson [1985] do not show this feature.

A third phase appears at ABU, SCO SH, LPZ, and COP SH that can be modeled as a third subevent occurring 16 s after the first subevent (Figure 8). The fact that this phase is seen at widely varying azimuths should rule out receiver structure as a possible cause of the phase, but a synthetic with three source-time functions does not fit the vertical components at SCO, COP, and PAR (Figure 8). A third subevent would increase the total moment of this earthquake to 5.3×10^{19} N m. The estimated geologic moment for this earthquake from slip along the Fairview fault is 4.5×10^{19} N m. If geologic moments for the West Gate and Gold King faults are included in the estimate, a total geologic moment of 5.5×10^{19} N m is obtained. Modeling of R2 and R3 recorded by a Pasadena strainmeter gives a moment of 1×10^{20} N m for the earthquake (D. I. Doser and H. Kanamori, unpublished manuscript, 1986). The geodetic model of Snay et al. [1985] also gives a moment value of 1×10^{20} N m for this earthquake.

December 16, 1954 (1111 UT) Dixie Valley (Event g)

Because the Dixie Valley earthquake (event g) occurred about 4 min after the Fairview Peak earthquake, it was

TABLE 2. Source Parameters From Body Wave Modeling

	Fault Zone	Mechanism Strike,Dip,Rake, deg	Focal Depth, km	Source-Time Function Rise,Plateau,Fall, s	Unilateral Rupture Length, km	$\Delta\sigma$, MPa	M_o^s, N m	$\hat{M}$
	June 6, 1954 (1113 UT)							
Event a	RM							6.2
subevent 1		336,80,-140(±5)	10±1	1,1.5,1 (±0.5)	7.5	1.4	1.3×10^{18}	
subevent 2		340,60,-115(±10)	7±2	1,1,1 (±0.2)	6.0	2.0	9.3×10^{17}	
	June 6, 1954 (2207 UT)							
Event b	RM	345,60,-135(±5)	8±2	1,1,1 (±0.2)	6.0	1.3	8.0×10^{17}	5.9
	Aug. 24, 1954 (0551 UT)							
Event c	RM							6.5
subevent 1		355,50,-145(±5)	12±1	2,1,2 (±0.5)	9.0	1.1	2.8×10^{18}	
subevent 2		355,50,-145(±10)	12±3	2,1,2 (±0.5)	9.0	0.9	2.4×10^{18}	
subevent 3		355,50,-145(±10)	12±3	2,1,2 (±0.5)	9.0	0.7	1.7×10^{18}	
	Dec. 16, 1954 (1107 UT)							
Event f	F							6.9*
subevent 1		350,60,-160(±3)	15±2	2,2,2 (±0.5)	12.0	3.3	1.4×10^{19}	
subevent 2		350,60,-160(±5)	15±3	2,2,2 (±0.5)	12.0	3.5	1.5×10^{19}	
subevent 3?		350,60,-160(±5)	15±3	2,2,2 (±0.5)	12.0	6.0	2.4×10^{19}	
	Dec. 16, 1954 (1111 UT)							
Event g	DV							6.7
subevent 1		350,50,-90(±20)	12±3	2,1,2 (±0.5)	9.0	1.9	5.0×10^{18}	
subevent 2		350,50,-90(±20)	12±3	2,1,2 (±0.5)	9.0	1.8	4.8×10^{18}	

* $\hat{M}$=7.2 if moment of third event is included.

difficult to pick P arrivals for the later event. The ISS location for the Dixie Valley earthquake was the same as the ISS epicenter for the Fairview Peak earthquake (Figure 1). Romney [1957] obtained an epicenter located at the northern end of the Dixie Valley fault (Figure 1) by using S and Lg arrivals in addition to P arrivals. Using only P arrivals, we obtained a location 30 km east of the large bend in the fault scarp, implying a bilateral rupture for this event. It is important to note, however, that the large error bars imply that our location is very poorly constrained.

The fault scarp produced along the Dixie Valley fault dipped 55°-75° in bedrock [Slemmons, 1957] with a maximum vertical offset of 2 m (Table 1). Strike-slip movement along the fault was generally small, except near the extreme southern end of the surface rupture, where 2 m of left-lateral displacement was observed [Slemmons, 1957]. Snay et al.'s [1985] model from geodetic data for the Dixie Valley fault (Table 4) is similar to the observed surface faulting.

Seismograms of the Dixie Valley earthquake (Figure 9) were difficult to model. First, phases from the Dixie Valley earthquakes were imbedded in the coda of the Fairview Peak earthquake. Second, later phases from the Fairview Peak earthquake often interferred with arrivals from the Dixie Valley event. Arrival times for phases from both earthquakes were estimated for each station. If the phases seen at the stations did not begin within ± 5 s of the predicted time of the Dixie Valley phase or if a Fairview Peak phase arrived within 40 s of the predicted Dixie Valley arrival, the record was not modeled. Third, the station distribution for this earthquake places all the observations

TABLE 3. Fault Parameters From Geologic Information

Fault Zone	Event	Rupture Length, km	Vertical Displacement, m	Horizontal Displacement, m*	Average Strike	Dip	M_o^g, N m
Dixie Valley	g	36 (22)	1.8		10	55-75E	1.8×10^{19}
Fairview	f	30 (28)	1.9	2.1	12	55-75E	4.5×10^{19}
Gold King	f?	12	0.6		10	W	4.1×10^{18}
Rainbow Mtn.	a	16	0.25		15	E	1.3×10^{18}
Rainbow Mtn.	c	25	0.45		15	E	5.1×10^{18}
West Gate	f	20	0.5	0.5	10	W	5.7×10^{18}

Rainbow Mountain parameters are from Tocher [1956]; all others are from Slemmons [1957]. Parentheses denote length of fault with displacement > 1 m.

*Positive horizontal displacement is dextral; positive vertical displacement is normal dip slip movement.

TABLE 4. Fault Parameters From Geodetic Information

Fault	Event	Length, km	Vertical Displacement, m*	Horizontal Displacement, m	Strike	Dip	Width, km
Fairview	f	50	2.3	2.9	9	57E	8
Fairview (shallow)	f	34	2.3	3.6	12	63E	5
Fairview (deep)	f	58	1.6	0.8	347	59E	20
Dixie Valley	g	42	2.4	-0.3	6	60E	15
Gold King-West Gate	f	23	0.5	1.3	7	70W	5
Rainbow Mtn. (five faults)	a,c	112	5.5	0.6	7	68E	7
Rainbow Mtn. (six faults)	a,c	35	0.4	0.6	13	35E	20

First parameters for Fairview fault are from Savage and Hastie [1969]; all others are from Snay et al. [1985].

*Positive vertical displacement is normal dip slip; positive horizontal displacement is dextral.

near the center of the dilatational quadrant. This caused poor resolution of the source mechanism. Large changes in strike or dip did not significantly change the waveform shape.

Since a focal mechanism could not be obtained from the limited first-motion data, the modeling process was started at 10° strike, 60° dip, and -90° rake, the average of the observed surface faulting. The best fit to the waveforms was for a strike of 350°, although the waveform shape was not altered by variations of ±20° in rake. The S waves are fit slightly better by a mechanism with a small component of left-lateral strike-slip motion.

Waveforms for the Dixie Valley earthquake were best modeled by a double source-time function with a focal depth of 12 km. Romney's [1957] estimate of 40 km for the focal depth thus appears to be in error, as previously noted by Okaya and Thompson [1985] and Savage [1965]. The seismic moment (Table 2) was half the geologic moment (Table 3).

March 29, 1959 (Event h)

The ISS location and our relocation for the March 23, 1959, earthquake (event h) are consistent with rupture along the southern end of the Dixie Valley fault. The focal mechanism from first-motion data for the earthquake shows a large component of dextral slip, and the strike of the eastward dipping nodal plane more closely aligns with the observed strike of faults at the surface.

Savage and Church [1974] found that leveling in 1967 implies 100 mm of slip across the Fairview Peak fault zone between 1955 and 1967. Miller [1967] examined the triangulation surveys of 1955, 1958, and 1966, and he suggests 150 mm of right-lateral motion across the southern part of Dixie Valley caused by slip along the fault or strain accumulation. It is possible that this observed horizontal and vertical movement may be related to the March 23, 1959, earthquake, since the focal mechanism and magnitude of the earthquake appear consistent with the direction and amount of movement observed between 1955 and 1967.

June 23, 1959 (1435 and 1504 UT) (Events i and j)

The June 1959 earthquakes (i, j) at the southwestern corner of the study area relocated 15 to 20 km southwest of the ISS locations. Both earthquakes were felt at a microwave tower 10 km south of the ISS locations [Seismological Notes, 1960]. The second earthquake (event j), although of smaller magnitude, caused considerable damage to the access road to the microwave site. Both the ISS and our relocations for the second earthquake are closer to the microwave site than the locations for the first event, supporting the intensity observations at this site.

The first June 1959 event (i) indicates that right-lateral oblique slip is occurring along faults in the southern part of the study area. The strike of the eastward dipping nodal plane more closely matches the observed trend of faults and structures in this area.

Discussion

Body wave modeling and first-motion data, coupled with geologic and geodetic information, reveal several important aspects of the fault geometry and faulting processes of this region.

First, all earthquakes of this sequence occurred along fault planes dipping 40° to 70°. There is no evidence of slip on listric or subhorizontal structures at depths less than 15 km in the Fairview Peak region, which are seen at shallow depths on seismic reflection profiles recorded in many parts of the Great Basin.

The rupture processes of the larger earthquakes ($M>6.5$) are complex and are characterized by bilateral faulting, multiple source time functions, fault orientations that vary with depth, and complicated patterns of surface faulting. With the exception of the Dixie Valley earthquake, the earthquakes of the sequence showed considerable strike-slip motion at depth, although the sense of motion at the surface was often dip-slip (events a and c). Multiple source-time functions and complex rupture patterns have previously been observed for earthquakes of the 1980 Mammoth Lake, California, sequence [T. C. Wallace, 1985; Lide and Ryall, 1985], the 1959 Hebgen Lake sequence [Doser, 1985], and the 1975 Yellowstone earthquake sequence [Bache et al., 1980]. All these earthquakes occurred in regions characterized by high levels of volcanic and magmatic activity. The Borah Peak earthquake, however, occurred in a region not associated with volcanic activity, and is best characterized by a simple source-time function with rupture along a planar fault [Doser and

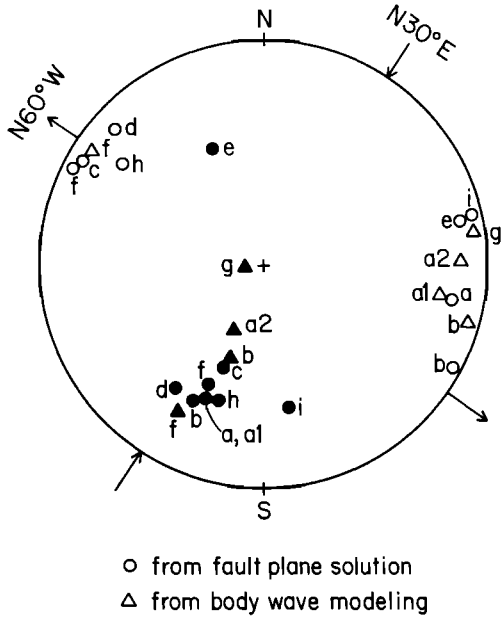

Fig. 10. P (solid symbols) and T axes (open symbols) of earthquakes from 1954-1959 from first-motion studies (circles) and body wave modeling (triangles). Arrows denote the orientation of the average regional stress (N60W extension, N30E compression) estimated by Ryall and Malone [1971].

Smith, 1985; Nabelek et al., 1985; Stein and Barrientos, 1985]. These observations lend support to the hypothesis that high-angle faulting in the Fairview Peak region may have been produced by magma movement or dike injection [Okaya and Thompson, 1985; Snay et al., 1985].

Body wave modeling indicates that the larger earthquakes nucleated in the same depth range (10 to 15 km) as the majority of microearthquakes [Stauder and Ryall, 1967], with the largest earthquakes ($M \geq 6.8$) nucleating at 12-15 km depth. Between 85% and 99% of all microearthquakes in the region occur above a depth of 16 km [Stauder and Ryall, 1967; Westphal and Lange, 1967], suggesting that the largest earthquakes occurred near the boundary of the brittle/ductile transition zone.

Vetter and Ryall [1983] have observed that earthquakes of $M_L < 5.0$ in the Fairview region exhibit changes in focal mechanism, with deeper (>9 km) events having oblique or normal slip mechanisms, and shallower (<9 km) events having predominately strike-slip mechanisms. They postulate that the change in mechanism is caused by increasing overburden pressure. This pattern of change is not observed in the five large earthquakes of 1954, suggesting that overburden pressure may play a limited role in controlling the faulting processes of $M > 6.5$ earthquakes.

Figure 10 compares a compilation of P and T axes from fault plane solutions and body wave modeling with the average direction of regional maximum extension (N 60° W) and compression (N30° E) as determined from the microearthquake studies of Ryall and Malone [1971] and the focal mechanism studies of Vetter and Ryall [1983]. Thompson and Burke [1973] have estimated a N50° W direction of maximum extension for the Dixie Valley from a study of fault grooves, and Savage [1983] estimated a direction of N74° W±11° from geodetic measurements. The P axes of Figure 10 show good agreement with the N30° E compression direction, although they do not plunge at 85° as observed by Ryall and Malone [1971] for microearthquakes. The tension axes are more scattered. This scatter is consistent with Ryall and Malone's [1971] observation that the fault zones in the region are a zig-zag series of fractures with varying strikes, that are moving in response to the same stress field. The net effect is that crustal blocks on the east sides of the fault zones are moving down and southwest with respect to the blocks on the western sides of the zones.

Ryall and Malone [1971] also used first-motion patterns and epicenter alignments of microearthquakes to further subdivide the Dixie Valley-Fairview fault zone into three smaller blocks, the Terminal zone, the Central zone, and the North zone (Figure 11). The average direction of maximum extension in each of these zones is shown in Figure 11. Wallace and Whitney [1984] consider the North zone to be the southernmost block of the Dixie Valley-Stillwater-Pleasant Valley fault zone based on studies of late Quaternary faulting. If we extend these zone boundaries to include the Rainbow Mountain fault zone, then the majority of earthquakes (events a, b, c, e, and f) between 1954 and 1959 occurred in the Central zone. The T axes of these earthquakes are in good agreement with the average direction of extension for the Central zone. Events d, g, and h in the North zone do not agree with the average extension direction obtained from microearthquakes but rather suggest a stress field similar to that of the Central zone. With the exception of event c, it appears that surface rupture during the individual earthquakes was confined to a single zone or block. Surface rupture during the 1903 Wonder earthquake also appears to have ruptured only within the North zone. Although event c appears to be an exception to the rupture patterns, most ground displacement during the earthquake was produced within the North zone. This grouping of displacement events along distinct blocks (the North and Central zones) while adjacent blocks have remained quiescent (the Terminal zone

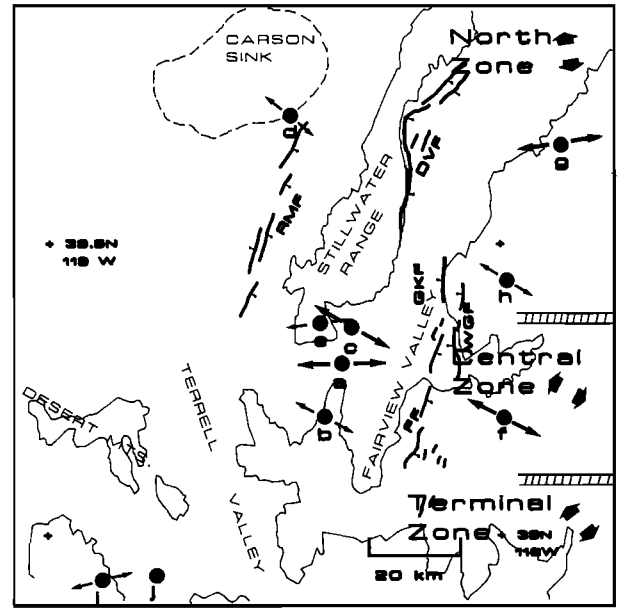

Fig. 11. Summary of earthquake processes in the Fairview Peak region. The right side of the figure shows the divisions of the Fairview-Dixie Valley fault zone as proposed by Ryall and Malone [1971]. The bold arrows on the right indicate the direction of extension in each of the zones as determined from microearthquake focal mechanisms [Ryall and Malone, 1971]. The dots denote earthquakes. Bold arrows near the earthquakes indicate the average extension direction from body wave and/or first-motion mechanisms.

and the Stillwater gap to the north of the North zone) has been observed along many faults within the intermountain region [Wallace and Whitney, 1984; R. E. Wallace, 1985; Schwartz and Coppersmith, 1984].

It is difficult to determine what east-west trending structures may control the segmentation of fault zones within this region. Stewart [1980] shows both Mesozoic age folding and an extensive Cenozoic volcano-tectonic trough striking across the region in an east-west direction, and these may have some influence on the segmentation.

Conclusions

This study has combined new information from seismic analysis with previous geodetic and geologic information to examine the earthquake processes in the Rainbow Mountain-Fairview Peak-Dixie Valley region between 1954 and 1959. Results of the study show (1) the earthquakes occurred along faults dipping 40° to 70°, (2) earthquakes of M>6.3 occurred at depths of 7 to 15 km with the M>6.8 events at depths of 12-15 km, (3) the larger earthquakes are best modeled with multiple source-time functions, with the exception of the July 6, 1954, aftershock, which appears to be a simple event, (4) P and T axes for focal mechanisms obtained from first-motion data and body wave modeling are consistent with an average regional extension direction of N60°W, (5) the distribution of faulting, epicenters, and focal mechanisms suggests that the region may be divided into three separate blocks with surface rupture during earthquakes primarily confined to a single block, and (6) afterslip seen along the Dixie Valley and Fairview faults between 1954 and 1960 may be related to the March 23, 1959, earthquake.

Comparisons of these earthquakes with the Borah Peak and Hebgen Lake earthquakes suggest that low-angle listric faults in the upper 15 km of the crust have not been activated by M>6.5 earthquakes in the intermountain region. The earthquakes of the Rainbow Mountain-Fairview Peak-Dixie Valley sequence showed considerably more complex rupture patterns than the Hebgen Lake and Borah Peak earthquakes, but their stress drops were comparable to the low (<15 MPa) stress drops observed for the more recent earthquakes. In the future we hope to examine the 1932 (M=7.2) Cedar Mountain, Nevada, and 1934 Excelsior Mountain, Nevada (M=6.5), earthquakes to determine whether features of the earthquake rupture process seen in the Fairview Peak region are similar to earthquake sequences in other parts of Nevada.

Acknowledgments. T. Webb provided a starting version of the body wave program that was modified and used in this analysis. M. R. Baker patiently digitized and redigitized seismograms as well as helping with aspects of the programming. S. Wesnousky critically reviewed an early version of the manuscript and offered helpful comments. Comments by A. Ryall, D. E. James, and an associate editor are also appreciated. D. Helmberger provided useful advice during the modeling process. The help of numerous people from around the world who provided seismograms for this study is also appreciated. D. Doser was supported by a Caltech Bantrell postdoctoral research fellowship during this study. Division of Geological and Planetary Science, California Institute of Technology, Pasadena, contribution 4296.

References

Aki, K., The use of Love waves for the study of earthquake mechanisms, J. Geophys. Res., 65, 323-340, 1960.

Allmendinger, R. W., J. W. Sharp, D. Von Tish, L. Serpa, L. Brown, S. Kaufman, J. Oliver, and R. B. Smith, Cenozoic and Mesozoic structure of the eastern Basin and Range Province, Utah, from COCORP seismic reflection data, Geology, 11, 532-536, 1983.

Anderson, R. E., M. L. Zoback, and G. Thompson, Implications of selected subsurface data on the structural form and evolution of some basins in the northern Basin and Range Province, Nevada and Utah, Geol. Soc. Am. Bull., 94, 1055-1072, 1983.

Bache, T. C., D. G. Lambert, and T. G. Barker, A source model for the March 28, 1975, Pocatello Valley earthquake from time-domain modeling of teleseismic P waves, Bull. Seismol. Soc. Am., 70, 405-418, 1980.

Cloud, W. K., Intensity distribution and strong-motion seismogram results, Nevada earthquakes of December 16, 1954, Bull. Seismol. Soc. Am., 47, 327-334, 1957.

Doser, D. I., Source parameters and faulting processes of the 1959 Hebgen Lake, Montana, earthquake sequence, J. Geophys. Res., 90, 4537-4555, 1985.

Doser, D. I., and R. B. Smith, Source parameters of the 28 October, 1983, Borah Peak, Idaho, earthquake from body wave analysis, Bull. Seismol. Soc. Am., 75, 1041-1051, 1985.

Fara, H. D., A new catalog of earthquake fault plane solutions, Bull. Seismol. Soc. Am., 54, 1491-1518, 1964.

Flinn, E. A., Confidence regions and error determinations for seismic event location, Rev.Geophysics, 3, 157-185, 1965.

Hanks, T. C., and H. Kanamori, A moment magnitude scale, J. Geophys. Res., 84, 2348-2350, 1979.

Hastings, D. D., Results of exploratory drilling, north Fallon Basin, western Nevada, in Basin and Range Symposium, edited by G. W. Newman and H. D. Good, pp. 515-522, Rocky Mtn. Assoc. Geol.-Utah Geol. Assoc., Denver, Colo., 1979.

Herrin, E., Seismological tables for P phases, Bull. Seismol. Soc. Am., 58, 1193-1239, 1968.

Kanamori, H., and G. S. Stewart, Mode of strain release along the Gibbs fracture zone, Mid-Atlantic Ridge, Phys. Earth Planet. Inter., 11, 312-332, 1976.

Langston, C. A., and D. V. Helmberger, A procedure for modeling shallow dislocation sources, Geophys. J. R. Astron. Soc., 42, 117-130, 1975.

Lide, C. S., and A. S. Ryall, Aftershock distribution related to the controversy regarding the mechanisms of the May 1980, Mammoth Lakes, California, earthquakes, J. Geophys. Res., 90, 11,151-11,163, 1985.

Meister, L. J., R. O. Burford, G. A. Thompson, and R. L. Kovach, Surface strain changes and strain energy release in the Dixie Valley-Fairview Peak area, Nevada, J. Geophys. Res., 73, 5981-5994, 1968.

Miller, R. W., Earthquake movement study in the vicinity of Fallon, Nevada, U.S. Coast and Geod. Surv. Rep. 564, U. S. Dep. of Commerce, Rockville, Md., 1967.

Nabelek, J., H. Eyidogan, and M. N. Toksoz, Source parameters of the Borah Peak, Idaho, earthquake of October 28, 1983 from body wave inversion (abstract), Eos Trans. AGU, 66, 308, 1985.

Okaya, D. A., and G. A. Thompson, Geometry of Cenozoic extensional faulting: Dixie Valley, Nevada, Tectonics, 4, 107-126, 1985.

Romney, C., Seismic waves from the Dixie Valley-Fairview Peak earthquakes, Bull. Seismol. Soc. Am., 47, 301-319, 1957.

Ryall, A., and S. D. Malone, Earthquake distribution and mechanics of faulting in the Rainbow Mountain-Dixie Valley-Fairview Peak area, central Nevada, J. Geophys. Res., 76, 7241-7248, 1971.

Savage, J. C., The stopping phase on seismograms, Bull. Seismol. Soc. Am., 55, 47-52, 1965.

Savage, J. C., Strain accumulation in the western United States, Ann. Rev. Earth Planet. Sci., 11, 11-43, 1983.

Savage, J. C., and J. P. Church, Evidence for post earthquake slip in the Fairview, Dixie Valley, and Rainbow Mountain fault areas of Nevada, Bull. Seismol. Soc. Am., 64, 687-698, 1974.

Savage, J. C., and L. M. Hastie, A dislocation model for the Fairview Peak, Nevada, earthquake, Bull. Seismol. Soc. Am., 59, 1937-1948, 1969.

Schwartz, D. P., and K. J. Coppersmith, Fault behavior and characteristic earthquakes: Examples from the Wasatch and San Andreas fault zones, J. Geophys. Res., 89, 5681-5698, 1984.

Seismological Notes, Bull. Seismol. Soc. Am., 50, 154-157, 1960.

Slemmons, D. B., Geologic setting for the Fallon-Stillwater earthquakes of 1954, Bull. Seismol. Soc. Am., 46, 4-9, 1956.

Slemmons, D. B., Geological effects of the Dixie Valley-Fairview Peak, Nevada, earthquakes of December 16, 1954, Bull. Seismol. Soc. Am., 47, 353-375, 1957.

Slemmons, D. B., K. V. Steinbrugge, D. Tocher, G. B. Oakeshott, and V. P. Gianella, Wonder, Nevada earthquake of 1903, Bull. Seismol. Soc. Am., 49, 251-256, 1959.

Smith, R. B., and R. L. Bruhn, Intraplate extensional tectonics of the eastern Basin-Range: Inferences on structural style from seismic reflection data, regional tectonics, and thermal-mechanical models of brittle-ductile deformation, J. Geophys. Res., 89, 5733-5762, 1984.

Smith, T. E., Aeromagnetic measurements in Dixie Valley, Nevada: Implications on Basin-Range structure, J. Geophys. Res., 73, 1321-1331, 1968.

Snay, R. A., M. W. Cline, and E. L. Timmermann, Dislocation models for the 1954 earthquake sequence in Nevada, USGS Open File Rep. 85–290, 531-555, 1985.

Starr, A. T., Slip in a crystal and rupture in a solid due to shear, Proc. Cambridge. Philos. Soc., 24, 489-500, 1928.

Stauder, W., and A. Ryall, Spatial distribution and source mechanisms of microearthquakes in central Nevada, Bull. Seismol. Soc. Am., 57, 1317-1345, 1967.

Stein, R. S., and S. E. Barrientos, Planar high-angle faulting in the Basin and Range: Geodetic analysis of the 1983 Borah Peak, Idaho, earthquake, J. Geophys. Res., 90, 11,355-11,366, 1985.

Stewart, J. H., Geology of Nevada, Spec. Publ. 4, 136 pp., Nev. Bur. of Mines and Geol., Reno, 1980.

Thompson, G. A., and D. B. Burke, Rate and direction of spreading in Dixie Valley, Basin and Range province, Nevada, Geol. Soc. Am. Bull., 84, 627-632, 1973.

Tocher, D., Movement on the Rainbow Mountain fault, Bull. Seismol. Soc. Am., 46, 10-14, 1956.

Vetter, U. R., and A. S. Ryall, Systematic change of focal mechanism with depth in the western Great Basin, J. Geophys. Res., 88, 8237-8250, 1983.

Wallace, R. E., Variations in slip rates, migration, and grouping of slip events on faults in the Great Basin province, USGS Open File Rep. 85–290, 17-26, 1985.

Wallace, R. E., and R. A. Whitney, Late Quaternary history of the Stillwater seismic gap, Nevada, Bull. Seismol. Soc. Am., 74, 301-314,1984.

Wallace, T. C., A reexamination of the moment tensor solutions of the 1980 Mammoth Lakes earthquakes, J. Geophys. Res., 90, 11,171-11,176, 1985.

Westphal, W. H., and A. L. Lange, Local seismic monitoring--Fairview Peak area, Nevada, Bull. Seismol. Soc. Am., 57, 1279-1298, 1967.

Whitten, C. A., Geodetic measurements in the Dixie Valley area, Bull. Seismol. Soc. Am., 47, 321-325, 1957.

Wickens, A. J., and J. A. Hodgson, Computer re-evaluation of earthquake mechanism solutions 1922-1962, Publ. 33, pp. 1-500, Dominion Observ., Ottawa, Ont., 1967.

D. I. Doser, Department of Geological Sciences, University of Texas at El Paso, El Paso, TX 79968.

(Received March 6, 1986;
revised June 27, 1986;
accepted July 29, 1986.)